INFRAGRAVITY WAVE PROPAGATION AND DISSIPATION ON A LOW-SLOPING LABORATORY BEACH

Anouk de Bakker[1], Marion Tissier[1], Vincent Marieu[2], Nadia Sénéchal[2], Andrea Ruju[3], Javier Lara[4] and Gerben Ruessink[1]

Abstract

An extensive new laboratory dataset, obtained on a 1:80 sloping fixed beach, is analyzed to obtain further insight into infragravity-wave propagation and dissipation. In our dataset, infragravity waves originate from the non-linear energy transfer from short waves. The previously reported change in phase lag of the infragravity waves behind the short wave group is also observed in our data, and induces a frequency-dependent infragravity growth rate during shoaling. Ultimately, negative zero-lag correlations with the short wave groups offshore of the surf zone change into positive correlations in shallow water, indicating depth modulation of the short waves by the infragravity waves. Ninety % of the incoming infragravity-wave energy is observed to dissipate, which initiates at the start of short-wave breaking. About half of that 90% is dissipated very close to shore (swash zone) potentially because of infragravity-wave breaking.

Key words: Infragravity waves, laboratory experiments, propagation, reflection coefficients, energy dissipation

1. Introduction

Infragravity waves are 20-200 s waves that may be important to beach and dune erosion (e.g. Russell, 1993; Van Thiel de Vries et al. 2008), as their energy can dominate the water motion very close to shore during storms (e.g. Guza and Thornton, 1982; Ruessink et al. 1998; Sénéchal et al. 2011). Infragravity waves can originate by two different mechanisms. The first mechanism is the non-linear energy transfer from short sea and swell (typically, 2-20 s) waves (e.g. Longuet-Higgins and Stewart, 1962; Herbers et al., 1994). The short waves force a second-order infragravity wave that well seaward of the surf zone is in anti-phase with the wave group and has the same wave length and period as the wave group. In the second mechanism, infragravity waves arise as set-up/down waves at the time-varying breakpoint of the grouped short waves (Symonds et al., 1982). In this mechanism both seaward and shoreward travelling infragravity are radiated from the outer edge of the short-wave surf zone. On steep slopes the time-varying breakpoint appears to be the dominant generation mechanism, while on lower-sloping beaches the non-linear energy transfer from short waves accounts completely for infragravity-wave generation (Battjes et al. 2004; Dong et al., 2009).

During short-wave propagation towards the shore, the short waves shoal and increase in height. The accompanying infragravity waves that are bound to the short wave groups are enhanced as well, up to the point of initial short wave breaking (e.g. List, 1992; Masselink, 1995), or even into the surf zone (Schäffer and Svendsen, 1988). Several studies indicate that bound infragravity waves shoal much stronger than free infragravity waves, which shoal according to Green's law ($H \sim h^{-1/4}$); here H is height and h is water depth. Battjes et al. (2004) concluded from laboratory experiments that the growth rate of the incoming infragravity waves increases considerably with frequency, being of the order of Green's law for the lower frequencies and comparable to the shallow-water limit ($H \sim h^{-5/2}$) of the Longuet-Higgins and Stewart (1962) equilibrium solution for the highest infragravity frequencies. This implies a frequency-dependent effectiveness of the transfer of energy between short waves and infragravity waves. Battjes et al. (2004) attributed this to the larger phase lag of the higher infragravity frequencies with the short wave envelope, a

[1] Dept. Physical Geography, Faculty of Geosciences, Utrecht University, Netherlands. a.t.m.debakker@uu.nl, m.f.s.tissier@uu.nl and b.g.ruessink@uu.nl.
[2] UMR EPOC, Université de Bordeaux I, France. v.marieu@epoc.u-bordeaux1.fr and n.senechal@epoc.u-bordeaux1.fr
[3] School of Marine Science and Engineering, Plymouth University, United Kingdom, andrea.ruju@plymouth.ac.uk
[4] Environmental Hydraulics Institute "IH Cantabria", Universidad de Cantabria, Spain. jav.lopez@unican.es

necessary condition for the energy transfer (see e.g. Van Dongeren et al. 1997, Janssen et al. 2003).

Over the last decades it was believed that infragravity waves reflect almost completely from the shore to display a cross-shore standing pattern. However, recent observations challenge this viewpoint as they demonstrated that infragravity waves can in fact dissipate considerably when travelling shoreward (e.g. Ruessink 1998, Sheremet et al. 2002, Battjes et al. 2004, Thomson et al. 2006; De Bakker et al., in review). Despite several field, laboratory and modeling studies dedicated to identifying the responsible dissipation mechanism, the specific dissipation mechanism(s) is(are) still unclear. Potential mechanisms include bottom friction (Henderson and Bowen, 2002), energy transfer from the infragravity to sea/swell frequencies (Thomson et al., 2006 and Henderson et al., 2006) and the breaking of the infragravity wave in very shallow water close to the shoreline due to self - self interactions (e.g. Battjes et al., 2004 and Van Dongeren et al., 2007). In this case the infragravity waves steepen up until they reach a limit and break. Recently, Ruju et al. (2012) suggested that both breaking and non-linear energy transfer might account for a part of the observed energy loss, but in different parts of the surf zone.

Here, we will use new laboratory observations on a planar 1:80 sloping beach to investigate outstanding questions in the cross-shore dynamics of infragravity waves.

2. Laboratory experiment

The laboratory data were obtained as part of the GLOBEX project (Ruessink et al., 2013), where a high-resolution data set (both in space and time) was collected on a low-sloping (1:80) fixed laboratory beach. The first 16.6 m of the flume was horizontal, with a mean water level of 0.85 m. At x = 16.6 m, the sloping bed started and intersected with the mean water level at $x \approx 84.6$ m. The experimental program comprised eight wave conditions: 2 monochromatic conditions, 3 bichromatic conditions, and 3 random wave conditions. Here, we will focus on the three random-wave cases that contained one intermediate- (A1; H_s = 0.1 m, T_p = 1.58 s) and one high-energy (A2; H_s = 0.2 m, T_p = 2.25 s) sea-wave condition, and one narrow-banded swell condition (A3; H_s = 0.1 m, T_p = 2.25 s). The deployed instruments included 21 wave gauges to measure sea-surface elevation, 7 electromagnetic flow meters to record cross-shore and vertical flow velocities, and 4 video cameras to study wave propagation and run-up. Each condition was run for 75 minutes with the gauges and the flow meters sampling at 128 Hz, followed by a rest period of about 15 minutes. After all wave conditions were completed, the instruments were repositioned and the conditions were repeated with the same wave paddle signal. Altogether, the conditions were each repeated 10 times, resulting in a total of 190 and 43 positions with water level and flow-velocity data, respectively. See Ruessink et al. (2013) for further details and initial data processing.

3. Results

3.1. Wave propagation

3.1.1. Wave height

Figures 1a and b show the significant wave heights of the short-wave (0.37-15 Hz for A1, and 0.26-15 Hz for A2 and A3) band H_s and the infragravity wave (0.01-0.37 Hz for A1, and 0.01-0.26 Hz for A2 and A3) band H_{inf}, respectively for the three random wave conditions. For the most energetic case (A2), the first short waves started breaking at $x \approx 44$ m, and intense breaking started at $x \approx 55$ m. Up to this point, H_{inf} increased, then remained constant from $x \approx 55$ m to $x \approx 75$ m, to finally reduce in the innermost part of the surf zone. H_{inf} in the two other less energetic cases displayed similar behavior, although the stretch of constant infragravity-wave height was restricted to a smaller cross-shore range, corresponding to the restricted surf-zone width at these conditions; also the decrease in very shallow water is absent or less pronounced.

Furthermore, Figure 1 displays the significant incoming and outgoing infragravity-wave heights calculated with the separation method of Guza et al. (1984). As this method constructs surface elevation time series using co-located wave gauges and velocity meters, these heights are available at fewer points than in Figures 1a and b. Similar to the cross-shore evolution of the total infragravity wave height, the

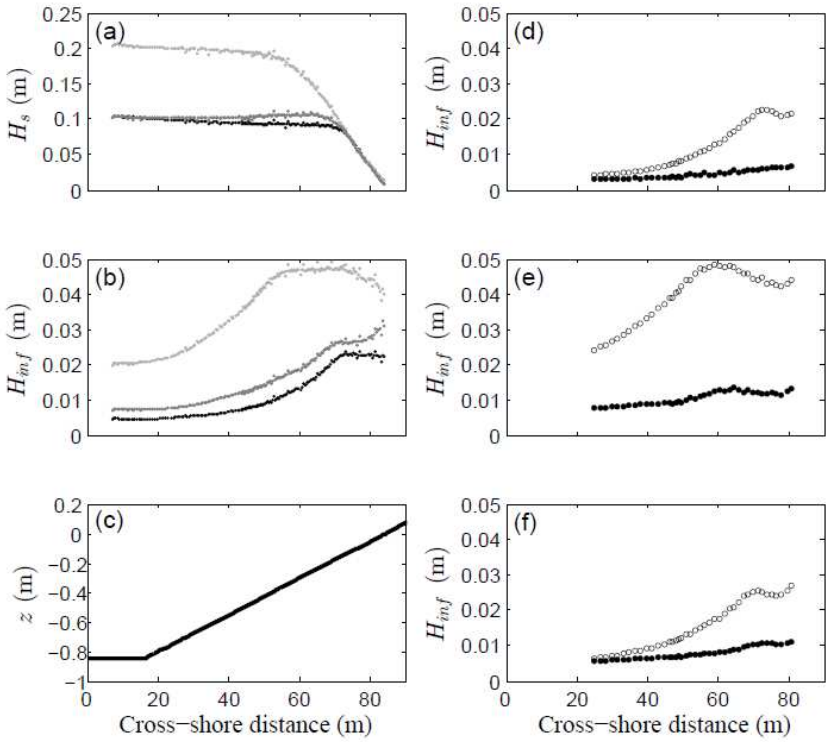

Figure 1. Significant wave height versus cross-shore distance x for (a) short waves H_s and (b) infragravity waves H_{inf} for A1 (black dots), A2 (light-grey dots) and A3 (dark-grey dots). (c) Bed profile. Furthermore, the significant incoming (circles) and outgoing (black dots) infragravity-wave heights calculated from separated signals (following Guza et al., 1984) are shown for (d) A1, (e) A2 and (f) A3.

incoming wave height increased until the start of the short-wave surf zone; further onshore the incoming wave height decreased somewhat, to finally increase close to the shoreline (x = 84.6 m). The substantial difference in incoming and outgoing infragravity wave height near the shoreline is striking, and is indicative of considerable infragravity-energy dissipation in very shallow water. We will further address this dissipation in Section 3.2.

3.1.2. Phase lag

To examine the growth of the infragravity energy over the sloping bed, we calculated the phase lag of the infragravity waves behind the short wave envelope A, where A is given by

$$A(t)=\left|\eta^{hf}(t)+i\Gamma\left\{\eta^{hf}\right\}\right|^{lf}, \tag{1}$$

where $\Gamma\{\}$ denotes the Hilbert transform operator. The phase lag φ of the surface elevation of the incoming infragravity waves, η_{in}, behind A, at frequency f is determined at position x as

$$\varphi_{m,x} = arctan\left(\frac{Im\left(Cr_{A\eta_{in}}(f,x)\right)}{Re\left(Cr_{A\eta_{in}}(f,x)\right)}\right), \tag{2}$$

where *arctan* is the arctangent of the imaginary (*Im*) part to the real part (*Re*) of the cross-spectrum of η_{in} and A, $Cr_{A\,\eta in}$. Figure 2 illustrates the phase lag of the incoming infragravity wave motion behind the short-wave envelope relative to the deep-water value of π (i.e. $\Delta\varphi = \varphi + \pi$) for the most energetic random wave condition (A2) at 5 different frequencies. The phase lag is seen to increase slightly in the shoreward direction for all infragravity frequencies, with the lowest frequencies experiencing a larger increase. The observed small phase lag in the short wave shoaling zone is necessary for an energy transfer from the short waves to the infragravity wave frequencies, thus allowing the infragravity waves to grow in height (see e.g.

Figure 1b) (see e.g. Van Dongeren et al. 1997, Janssen et al. 2003). Our observations that the lower frequencies show a larger increase in phase lag contradict the findings in Battjes et al. (2004), who observed $\Delta\varphi$ at the highest infragravity frequencies to increase considerably more than $\Delta\varphi$ at the lower infragravity frequencies. This frequency-dependent phase lag affects the shoaling rates, which will be discussed in the next subsection. The dashed line in Figure 2 is the location where all short waves were observed to break. Here the group structure has completely disappeared and coincides with a jump in phase difference from about 0 to ± 1.5 π. The increase to values above π agrees with the positive zero lag correlation between the short-wave envelope and the infragravity wave, which was reported several times for the surf zone (e.g. Janssen et al. 2003, Battjes et al. 2004, Van Dongeren et al. 2007).

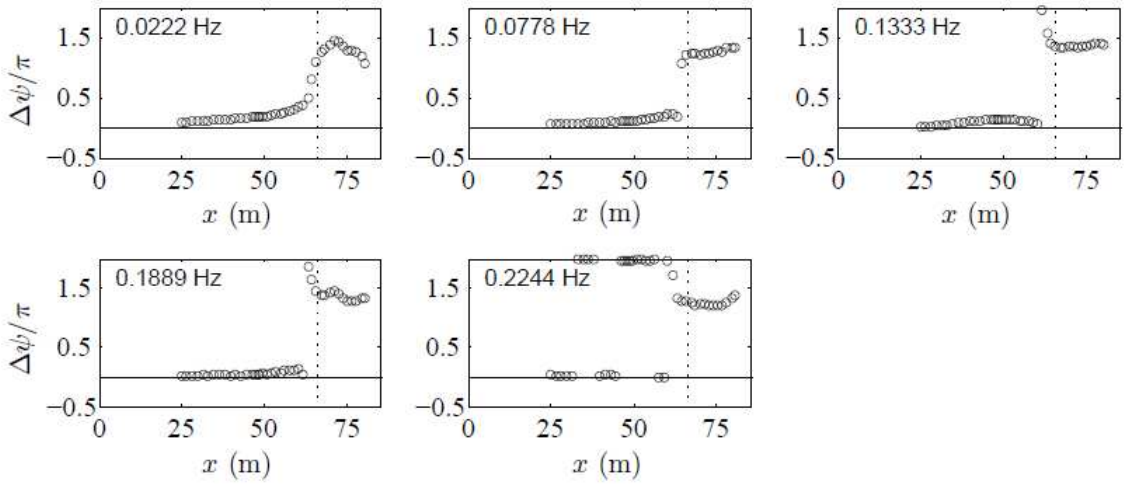

Figure 2. Additional phase lag ($\Delta\varphi$) of the infragravity wave behind the short wave envelope for 5 different frequencies for condition A2. The dashed line in the figures is the location where all short waves were observed to break.

3.1.3. Shoaling

Figure 3 shows the significant incoming and outgoing infragravity wave heights for three infragravity wave frequencies, plotted together with Green's law and the shallow-water asymptote of the Longuet-Higgins and Stewart (1962) equilibrium solution. Case A3 is shown here because of the low wave-steepness, so the shoaling trend is well visible. In the figure, the incoming wave height is seen to increase considerably when propagating towards the shore; however, the shoaling is less than predicted from the shallow water asymptote of the Longuet-Higgins and Stewart (1962) equilibrium solution. The growth rate of the lowest infragravity frequency is clearly larger than that for the higher infragravity frequencies. This is consistent with the observed slightly larger phase lag for the lower frequencies (see Figure 2), which allows more energy to be transferred to those frequencies, as suggested by Battjes et al. (2004).

The outgoing waves are seen to de-shoal, roughly following the predictions for free long waves (Green's law), although a relatively large offset exists close to shore, especially at the lowest infragravity frequency. Instead of shoaling until the shoreline, the infragravity waves arrest shoaling at the same time as the short waves. What has to be noted is that the assumptions of the separation technique of Guza et al. (1984) might no longer be valid in very shallow water (e.g. suitability of linear wave theory), which would affect the trends we observed.

3.1.4. Correlation with the short wave envelope

In Figure 4 the correlations (r) between the short-wave envelope A with a zero-mean, and the incoming, outgoing and total infragravity wave signal with a zero-mean, η_{inf}, were calculated following

$$r(\tau) = \frac{\langle \eta_{inf}(t) A(t+\tau) \rangle}{\sigma_{inf}\sigma_A}, \tag{3}$$

where $\langle .. \rangle$ denotes the time averaging operator, t is time and τ is a time shift. The σ_{inf} and σ_A are the

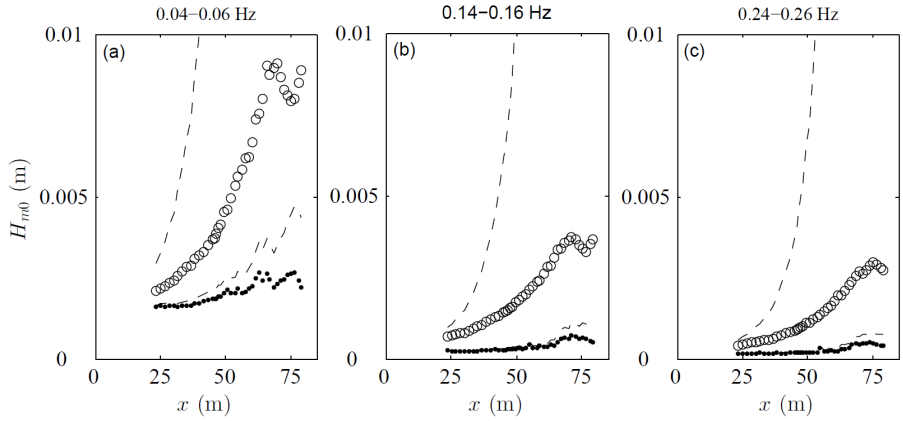

Figure 3. Incoming (circles) and outgoing (black dots) significant infragravity wave height for three frequency bands of case A3, (a) 0.04-0.06 Hz, (b) 0.14-0.16 Hz and (c) 0.24-0.26 Hz. Green's law (lower dashed line) and the shallow-water asymptote of the Longuet-Higgins and Stewart (1962) equilibrium solution (upper dashed line).

standard deviations of η_{inf} and A, respectively, and $-1 \leq r \leq 1$. A statistical analysis following Garrett and Toulany (1982) shows that values for r smaller than -0.1 and larger than 0.1 are significant for all conditions, except for outgoing waves at case A2 at $x < 75$ m where the critical level is at 0.2 to 0.5.

As can be seen in Figure 4, the short-wave envelope and the total infragravity wave signal were negatively correlated at $\tau = 0$ offshore of the short wave surf zone for all three random wave conditions, as can be expected for bound infragravity waves. The correlation starts to weaken where the largest short waves started to break. Onshore of the location where all short waves broke, the correlation was positive. This positive correlation is indicative of the depth modulation of the short waves by the infragravity waves. The infragravity wave crest locally increases the water depth, and so the slightly larger short waves can prevail, while at the infragravity wave trough the water depth is shallower and only small short waves are present, see also Tissier et al. (2013).

The correlation with only the incoming infragravity wave signal was slightly stronger than the total infragravity wave signal outside of the surf zone. The correlation with the outgoing infragravity wave was weak (≈ 0) at $\tau = 0$, as expected.

To explore the propagation of the infragravity wave and its relation with the short wave group in more detail, the cross correlations for $-180 < \tau < 180$ s are provided in Figure 5. The predicted travel time for the short-wave group to reach the shore and for the reflected infragravity waves to travel back offshore are shown too, calculated as described by Ruju et al. (2012),

$$F(\tau,x) = \int_x^0 \left(\frac{1}{c_g} + \frac{1}{c} \right) dx - \tau = 0 \,, \tag{4}$$

where c_g is the group speed and c is the propagation speed of waves in shallow water $\sqrt{gh}$. A statistical analysis following Garrett and Toulany (1982) shows that correlations smaller than -0.1 and larger than 0.1 are significant for cases A1 and A2, for A3 this is at values smaller than -0.2 and larger than 0.2.

Figures 5a-c provide the cross correlations of the total infragravity-wave signal at the most seaward location (x = 5.6 m) with the total infragravity-wave signal at all locations, for all three random wave conditions. The bars of high positive correlation extended from x = 5.6 m (at $\tau = 0$) all the way to the most shoreward station (x = 84.6 m). However, in the short-wave surf zone the correlation weakened, which is probably due to the dissipation of the incoming infragravity wave. The reflected infragravity signal was therefore not strongly correlated with the incoming signal, except for the low-wave steepness case A3. Overall, intermediate-energy case A1 shows the weakest correlations. Janssen et al. (2003) did not observe a weakening relation in the short-wave surf zone, and observed a strong correlation with the outgoing wave. This is most likely because of the much lower wave-steepness of their wave signal (H_s = 0.1 m, T_p = 3.33 s), and the steeper bed slope (~1:55) that cause less infragravity-wave energy to dissipate.

A small mismatch is visible between the bar of positive correlation of the incoming infragravity waves

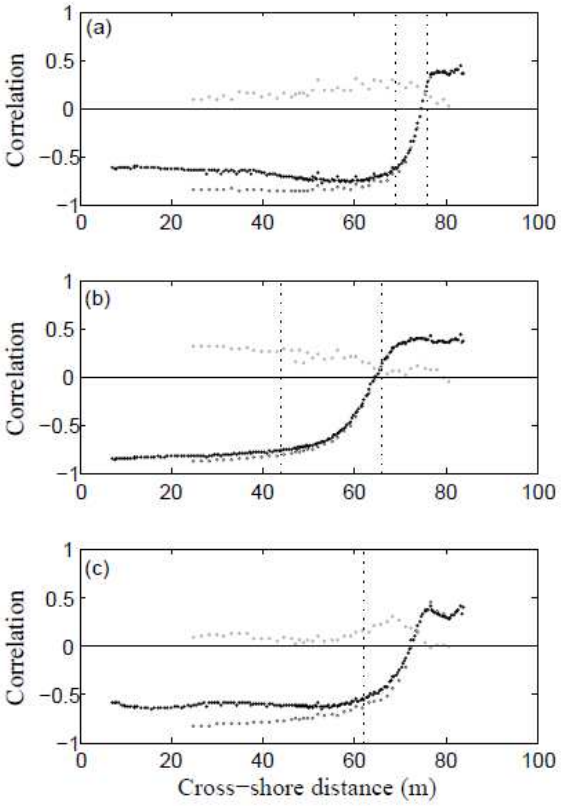

Figure 4. Correlations r at $\tau = 0$ between the short-wave envelope and the separated and total infragravity wave signal (a) A1, (b) A2 and (c) A3 with total infragravity wave signal (black dots), incoming infragravity wave signal (dark-grey dots) and outgoing infragravity wave signal (light-grey dots). Dashed lines are the visually determined location where (left) the largest short waves started to break, and (right) where all waves broke. The single line in (c) shows the initiation of short wave breaking, due to the narrow-banded spectrum the waves break close together.

with the computed time lag values. The gradient of the bar corresponding to the observed infragravity wave signal is slightly smaller than that of c_g. The correlation bar corresponding to the reflected infragravity waves is well represented by $\sqrt{gh}$. The asymmetric 'M' like pattern is formed by multiple correlations of the incoming signal with the reflected signal. Janssen et al. (2003) offer a detailed explanation for this pattern.

The cross correlations between the squared short wave envelope at one fixed location (x = 5.6 m) and the infragravity wave motion at every location (Figures 5d-f) show that a bar of strong negative correlation is following the predicted time lag values perfectly in the shoaling zone. However, closer to shore a small mismatch is visible, similar to the mismatch we saw earlier in Figures 5a-c. In the short-wave surf zone the initial strong negative correlation weakens due to energy dissipation of the infragravity waves. The absence of a set-down wave radiated from the outer surf zone and the fact that the cross correlation is negative until the shoreline, exclude any influence of the breakpoint mechanism in the generation of infragravity-wave energy in our data set. Instead the infragravity waves can be seen to reflect only at the shoreline.

In the zone where the short waves are breaking, a bar of stronger positive correlation is also present (at a more negative time lag) (Figures 5d-f). Janssen et al. (2003) hypothesize that the positive correlations are due to the presence of free waves that are positively correlated with the short-wave envelope. In Figures 5a-c this bar is present as well, but then as one of negative correlation.

3.1.5. EOF analyses

To explore the earlier observed frequency-dependent cross-shore infragravity-wave pattern, we performed a frequency-domain Complex Empirical Orthogonal Function (EOF) of the sea-surface elevations in the infragravity frequency band as outlined in Henderson et al. (2000). In figure 6, three frequencies are shown for the infragravity wave band during A2. The upper plots (Figures 6a-c) show the non-dimensional

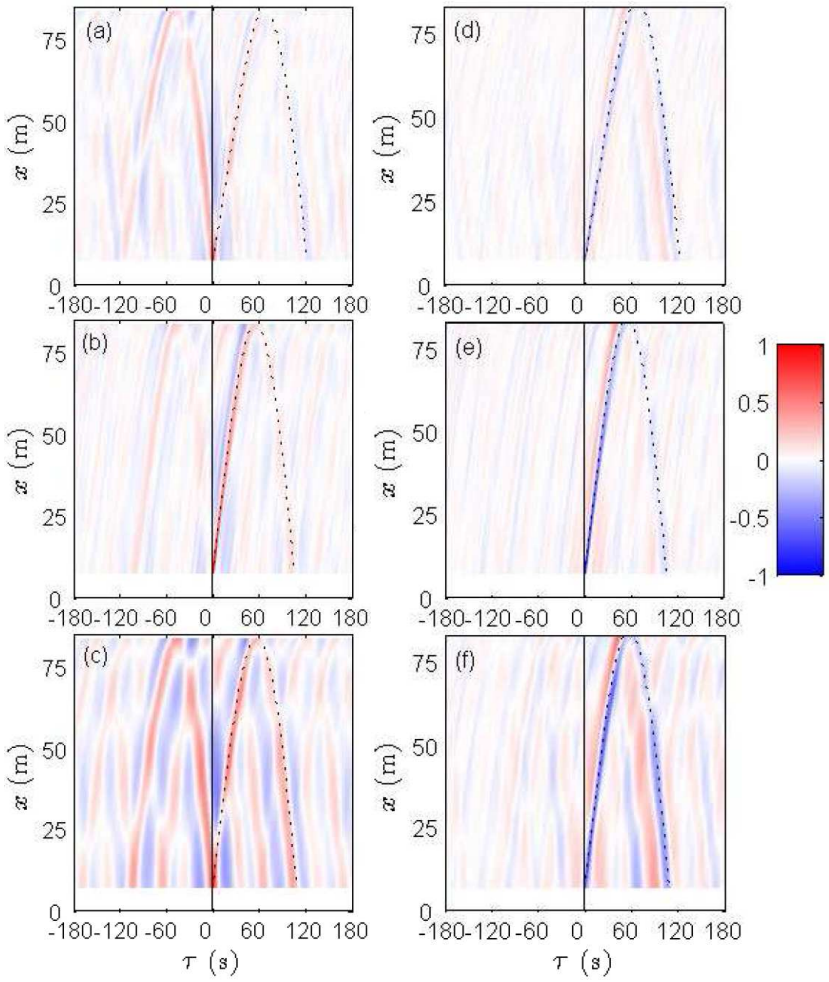

Figure 5. Correlation functions of the infragravity wave at all positions to a fixed reference position x = 5.6 m (a) A1, (b) A2, and (c) A3, and cross-correlation functions between the squared short wave envelope at a fixed reference position x = 5.6 m and the infragravity wave as observed at all locations (d) A1, (e) A2, and (f) A3. The solid line represents time lag (τ) is zero. Dashed lines indicate time lag values (calculated as described in Ruju et al., 2012) for shoreward propagating waves at group speed c_g, and in the offshore direction at $\sqrt{gh}$. Red colors indicate positive correlations, blue colors indicate negative correlations.

amplitude S, and the lower plots (Figures 6d-f) show the accompanying phases. For f = 0.0222 Hz, S shows a rather well-developed (anti)nodal structure, with nodes at $x \approx 35$ m and $x \approx 75$ m and antinodes at $x \approx 15$ m and $x \approx 60$ m which is indicative of a standing wave pattern. However the phases show no clear phase jump at the nodes (as expected for standing waves), but rather a combination of a phase jump and a monotonic increase towards the shore. At the higher infragravity frequencies (Figures 6b and 6c), the anti-nodal structure has disappeared, and the phases increase monotonically towards the shore. In general, only infragravity waves with frequencies smaller than 0.05 Hz (period $T > 20$ s) show any indication of a cross-shore standing pattern. This confirms that, due to the strong energy dissipation, the infragravity-wave field in the flume is largely dominated by onshore progressive waves. For the less-energetic cases A1 and A3, the transition from standing to progressive waves is at somewhat higher infragravity frequencies ($f \approx$ 0.0667 Hz), indicating overall less extensive energy dissipation.

3.2. Energy dissipation

To further investigate the cross-shore dissipation pattern of the infragravity wave, energy fluxes and corresponding reflection coefficients were calculated. For the calculation of incoming and outgoing frequency dependent energy fluxes ($F^{+}(f)$ and $F^{-}(f)$) the local method of Sheremet et al. (2002) was used. It

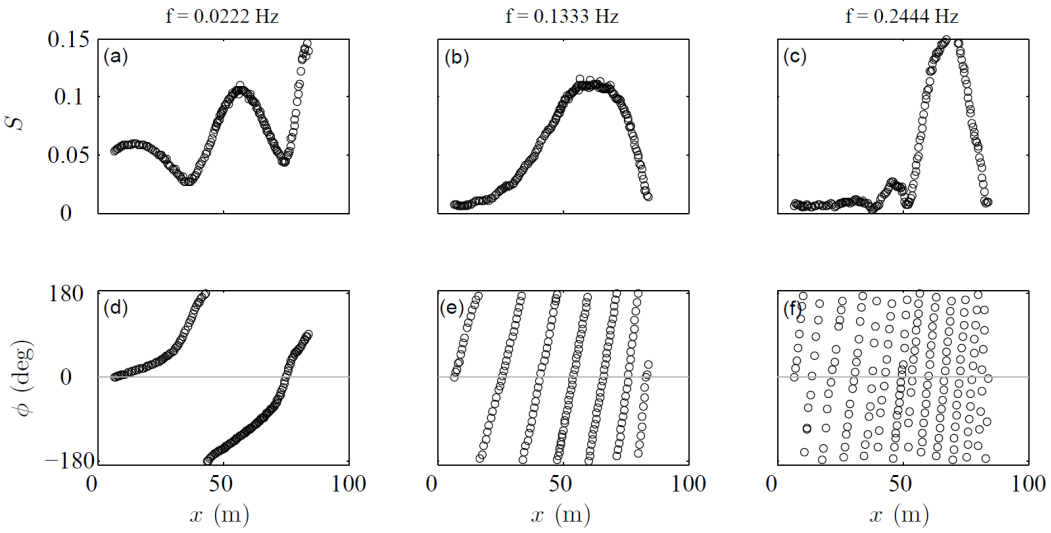

Figure 6. (a-c) Non-dimensional amplitude *S* and (d-f) phase φ for A2 were computed from the dominant Empirical Orthogonal Function of the cross-spectral matrix for each period. The cross-spectra were computed from 50% overlapping, Hamming-windowed series.

requires sea-surface elevation and cross-shore velocity as input. The energy (E) and cross-shore energy fluxes were calculated as

$$E^{\pm}(f) = \frac{1}{4}\left[Co_{\eta\eta}(f) + \frac{h}{g} Co_{uu}(f) \pm \left(2\sqrt{\frac{h}{g}} \right) Co_{\eta u}(f) \right], \tag{5}$$

$$F^{\pm}(f) = E^{\pm}(f)\sqrt{gh}, \tag{6}$$

where $Co_{\eta u}$ is the η-u cospectrum and $Co_{\eta\eta}$ and Co_{uu} are η and u autospectra, respectively (η is sea-surface elevation, u is cross-shore velocity). By integrating over the infragravity frequency range, bulk infragravity fluxes were computed,

$$F^{\pm} = \int_{f_{min}}^{f_{max}} F^{\pm}(f)\, df. \tag{7}$$

Reflection coefficients (R^2) were subsequently calculated from the incoming and outgoing energy flux as

$$R^2 = F^{-}/F^{+}. \tag{8}$$

Fluxes and reflection coefficients were calculated for the same frequencies as shown earlier in the EOF-plot (Figure 6) and confirm that the lowest infragravity frequencies (f < 0.05 Hz) conserve a large part of their energy, R^2 ~ 0.5, and therefore show a standing wave pattern, whereas the higher frequencies of the infragravity wave band undergo very strong energy dissipation. When integrated over all frequencies, the incoming infragravity energy flux is shown to increase up to the short wave surf zone, and then decrease strongly at the same time as the short waves (Figure 7a). Over a stretch of some 25 m, to a point just shoreward of the swash zone, about 50% of the total infragravity energy dissipated. The remaining 50% was almost completely dissipated in the zone shoreward of it, in the swash zone. There is barely any reflection from the shoreline (Figure 7b). The dissipation in very shallow water, and the narrow stretch over which it occurs, seems to indicate that wave breaking is the dominant dissipation source (e.g. Van Dongeren et al., 2007). This seems to be confirmed by the asymmetric bore shape of the infragravity waves just seaward of the swash, see also Ruessink et al. (2013).

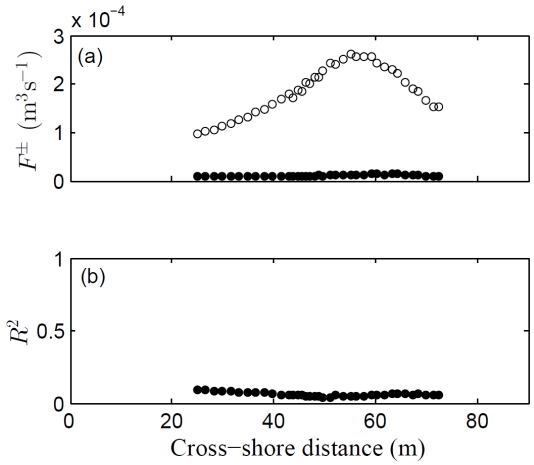

Figure 7. (a) Bulk incoming (circles) and outgoing (black dots) infragravity energy fluxes ($F^{\pm}$) for A2 and (b) bulk reflection coefficients (R^2) for the infragravity wave band for A2.

4. Discussion and Conclusion

In our data set infragravity waves are formed by nonlinear energy transfer from short waves, as incoming bound infragravity waves are present offshore of the short-wave surf zone and no additional offshore travelling wave is originated from the surf zone itself, which would have been indicative of the time-varying breakpoint mechanism. The phase lag of the infragravity wave behind the short-wave envelope increases slightly towards the shore. This phase lag is slightly larger at lower infragravity frequencies, contrasting with earlier studies that reported a slightly larger phase lag at higher infragravity frequencies. The phase lag is a necessary condition for energy transfer from the short waves to the infragravity wave. The slightly larger phase lag for the lower infragravity frequencies in our data results therefore in a stronger growth at those frequencies during shoaling. The growth of the infragravity waves ceases at the start of the short wave surf zone, from whereon the infragravity wave height stays constant until very close to the shoreline where it decreases.

Offshore of the short-wave surf zone the zero-lag correlation of the total and incoming infragravity wave signal with the short wave envelope is negative, indicative of bound waves in anti-phase with the short-wave group. In the short-wave surf zone the correlation weakens and shifts to a positive correlation. In very shallow water the correlation is positive due to the depth modulation of the short waves by the infragravity wave. The outgoing infragravity waves have a weak relation with the short-wave group. In the surf zone, the cross correlations between the squared short-wave envelope at one fixed location (x = 5.6 m) and the infragravity wave motion at every location show a bar of strong positive relation alongside of the incoming wave bars; this might indicate the release of the bound infragravity waves and the appearance of free waves. The cross correlations of the reflected infragravity-wave signal with the offshore squared short-wave envelope are very weak due to the strong infragravity energy dissipation.

The large energy dissipation of the infragravity wave results in a predominantly progressive cross-shore wave pattern. The bulk infragravity-wave energy fluxes increase up to the point of initial short-wave breaking, and from thereon decrease. About half of the total infragravity-wave energy is lost in the short-wave surf zone, and almost all the remaining infragravity-wave energy dissipates in the short stretch close to the shoreline. Reflection coefficients are therefore low. The fact that the energy dissipates over a very short stretch might indicate the breaking of the infragravity wave, which corresponds with the bore type shape of the wave just seaward of the swash.

Acknowledgements

Supported by the European Community's Seventh Framework Programme through the grant to the budget

of the Integrated Infrastructure Initiative Hydralab IV, Contract no. 261520. Anouk de Bakker and Gerben Ruessink acknowledge additional funding by the Netherlands Organisation for Scientific Research (NWO) under contract 821.01.012.

References

Battjes, J.A., Bakkenes, H.J., Janssen, T.T. and van Dongeren, A.R., 2004. Shoaling of subharmonic gravity waves, *Journal of Geophysical Research*, 109, doi: 10.1029/2003JC001863.

De Bakker, A.T.M., Tissier, M.F.S and Ruessink, B.G., *under review*. Shoreline dissipation of infragravity waves, *Continental Shelf Research*.

Dong, G., Ma, X., Xu, J., Ma, Y. and Wang, G., 2009. Experimental study of the transformation of bound long waves over a mild slope with ambient currents, *Coastal Engineering*, 56: 1035-1042.

Elgar, S., Herbers, T.H.C., Okihiro,M., Oltman-Shay, J. and Guza, R.T., 1992. Observations of infragravity waves, *Journal of Geophysical Research*, 97(C10), 15573-15577.

Garrett, C. and Toulany, B., 1982. Sea level variability due to meteorological forcing in the northeast Gulf of St. Lawrence, *Journal of Geophysical Research*, 87(C3), 1968-1978, doi: 10.1029/JC087iC03p01968.

Guza, R.T., Thornton, E.B., 1982. Swash oscillations on a natural beach, *Journal of Geophysical Research*, 87: 483–491.

Guza, R.T, Thornton, E.B. and Holman, R.A., 1984. Swash on steep and shallow beaches. *Proceedings* 19*th international Conference on Coastal Engineering*, ASCE, 708-723.

Henderson, S.M., and Bowen, J.A., 2002. Observations of surf beat forcing and dissipation. *Journal of Geophysical Research*, 107, doi:10.1029/200JC000498.

Henderson, S.M., Guza, R.T., Elgar, S., Herbers, T.H.C., and Bowen, A.J., 2006. Nonlinear generation and loss of infragravity wave energy, *Journal of Geophysical Research*, 111, doi:10.1029/2006JC003539.

Herbers, T.H.C., Elgar, S. and Guza, R.T., 1994. Infragravity-frequency (0.005-0.05 Hz) motions on the shelf. Part I: forced waves, *Journal of Physical Oceanography*, 24: 917-927.

Janssen T.T. and Battjes, J.A., 2003. Long waves induced by short-wave groups over a sloping bottom. *Journal of Geophysical Research*, 108, doi:10.1029/2002JC001515.

List, J.H., 1992. A model for two-dimensional surfbeat, *Journal of Geophysical Research*, 97: 5623-5635.

Longuet-Higgins, M.S. and Stewart, R.W., 1962. Radiation stress and mass transport in gravity waves with application to "surf-beats", *Journal of Fluid Mechanics*, 8: 565-583.

Masselink, G., 1995. Group bound long waves as a source of infragravity energy in the surf zone, *Continental Shelf Research*, 15(13): 1525-1547.

Ruessink, B.G., 1998. The temporal and spatial variability of infragravity energy in a barred nearshore zone, *Continental Shelf Research*, 18: 585-605.

Ruessink, B.G., Michallet, H., Bonneton, P., Mouazé, D. Lara, J.L., Silva, P.A., and Wellens, P., 2013. GLOBEX: Wave dynamics on a gently sloping laboratory beach, *Proceedings of the Conference on Coastal Dynamics*.

Ruju, A., Lara, J.L. and Losada, I.J., 2012. Radiation stress and low-frequency energy balance within the surf zone: A numerical approach, *Coastal Engineering*, 68: 44-55.

Russell, P., 1993. Mechanisms for beach erosion during storms. *Continental Shelf Research*, 13: 1243-1265.

Schäffer, H.A., and Svendsen, I.A., 1988. Surf beat generation on a mild-slope beach, *Coastal Engineering*, 1058-1072.

Sénéchal, N., Coco, G., Bryan, K.R., Holman, R.A., 2011. Wave runup during extreme storm conditions, *Journal of Geophysical Research*, 116, C07032, doi:10.1029/2010JC006819.

Sheremet, A., Guza, R.T., Elgar, S. and Herbers T.H.C., 2002. Observations of nearshore infragravity waves: Seaward and shoreward propagating components, *Journal of Geophysical Research*, 107, doi:10.1029/2001JC000970.

Symonds, G., Huntley, D. and Bowen, A.J., 1982. Two-dimensional Surf Beat: Long wave generation by a time-varying breakpoint, *Journal of Geophysical Research*, 87: 492-498.

Thomson, J., Elgar, S., Raubenheimer, B., Herbers, T.H.C. and Guza, R.T., 2006. Tidal modulation of infragravity waves via nonlinear energy losses in the surf zone, *Geophysical Research Letters*, 33, doi:10.1029/2005GL025514.

Tissier, M., Almar, R., Bonneton, P., Michalet, H., Birrien, F., de Bakker, A. and Ruessink, G., 2013. Individual wave celerity in the surf zone of a low-sloping laboratory beach, *Proceedings of the Conference on Coastal Dynamics*.

Van Dongeren, A.R. and Svendsen, I.A., 1997. Quasi 3-D modeling of nearshore hydrodynamics, *Research Report No. CACR-97-04, Center for Applied Coastal Research, University of Delaware*.

Van Dongeren, A.R., Battjes, J., Janssen, T., van Noorloos, J., Steenhauer, K., Steenbergen, G. and Reniers, A., 2007. Shoaling and shoreline dissipation of low-frequency waves, *Journal of Geophysical Research*, 112, doi:10.1029/2006JC003701.

Van Thiel de Vries, J.S.M., van Gent, M.R.A., Walstra, D.J.R., Reniers, A.J.H.M., 2007. Analysis of dune erosion processes in large-scale flume experiments, *Coastal Engineering*, 55: 1028–1040.